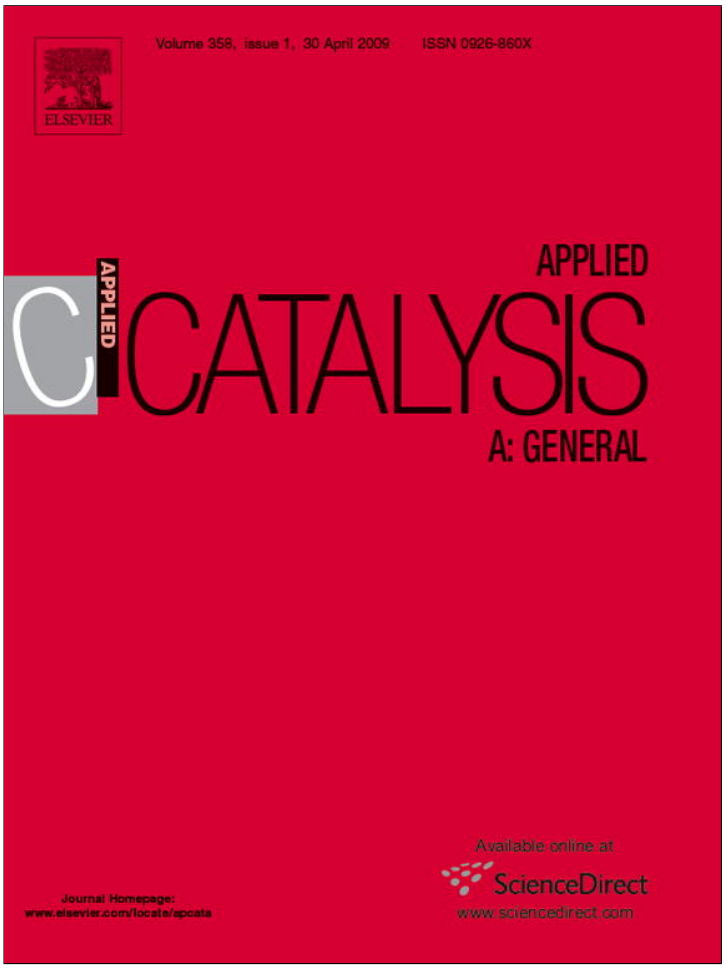

Applied Catalysis A: General 358 (2009) 95–102

Contents lists available at ScienceDirect

Applied Catalysis A: General

journal homepage: www.elsevier.com/locate/apcata

# Ionone synthesis by cyclization of pseudoionone on silica-supported heteropolyacid catalysts

V.K. Díez, B.J. Marcos, C.R. Apesteguía, J.I. Di Cosimo *

*Catalysis Science and Engineering Research Group (GICIC), INCAPE, UNL-CONICET. Santiago del Estero 2654. (3000) Santa Fe, Argentina*

ARTICLE INFO

*Article history:*
Received 20 October 2008
Received in revised form 3 February 2009
Accepted 5 February 2009
Available online 12 February 2009

*Keywords:*
Ionone
Heteropolyacid
Acid catalysis
Tungstophosphoric acid
HPA

ABSTRACT

The liquid-phase cyclization of pseudoionone to ionones (α, β and γ isomers) was studied on silica-supported heteropolyacid (HPA) catalysts containing between 18.8 and 58.5% HPA. The HPA used was tungstophosphoric acid ($H_3PW_{12}O_{40}$). The catalyst surface and structural properties were thoroughly characterized by several techniques. The density, chemical nature and strength distribution of the surface acid sites were determined by adsorbing and monitoring by temperature-programmed desorption and infrared spectroscopy probe molecules such as $NH_3$ and pyridine. The pseudoionone conversion to ionones increased linearly with the Brønsted acid site density until the HPA loading approached to the monolayer saturation coverage. For higher HPA contents, the pseudoionone adsorption and conversion were hampered because of spatial constraints that diminished the reactant accessibility to the proton active sites. The highest ionone yield, 79%, was obtained on a 58.5 wt% HPA/$SiO_2$ catalyst at 383 K and is comparable to the best values reported in literature for the homogeneously catalyzed reaction using sulfuric acid. The ionone isomer distribution was modified by varying both the temperature and the reaction time. A reaction mechanism was postulated in which ionone isomers (α, β and γ) are primary products, but γ-ionone is isomerized to α-ionone while β-ionone is not converted in the other isomers.



## 1. Introduction

Ionones (α, β and γ isomers) are extensively used as pharmaceuticals and fragrances. In particular, β-ionone is the preferred reactant for different synthesis processes leading to vitamin A while α- and γ-ionones are very appreciated in the fragrance industry because of their violet and woody-fruity scent, respectively [1,2].

The current commercial synthesis of ionones from citral takes place via a homogeneously catalyzed two-step process, as depicted in Scheme 1. The first step is the aldol condensation of citral with acetone to give pseudoionone (PS). Then, the consecutive cyclization of PS to ionones is catalyzed by strong mineral acids [3]. The ionone isomer distribution is determined by the acid catalyst nature, concentration and strength. For instance, concentrated sulfuric acid produces predominantly β-ionone [4–6] while phosphoric acid forms essentially α-ionone [3], and a Lewis acid such as $BF_3$ is required for γ-ionone synthesis [7].

However, the use of mineral bases and acids in Scheme 1 entails concerns related to high toxicity, corrosion, and disposal of spent catalysts. There is, therefore, a clear interest for developing more ecofriendly synthesis routes to produce ionones, in particular using solid catalysts. In this regard, several papers have been lately published on the use of solid bases to catalyze the first reaction step of Scheme 1, reporting PS yields of about 90% [8–11]. In contrast, very few works have focused on the use of solid acids for PS cyclization to ionones (second reaction step of Scheme 1) [4,5,6]. Moreover, the reported ionone yields on solid acids are still significantly lower than those obtained via the homogeneous reaction (80–90%). For example, strongly acidic resins and sulfated and persulfated $TiO_2$/MCM-41 yield 30–49% ionones by PS cyclization [12,13].

In a previous work [14], we explored the liquid-phase cyclization of PS to ionones on several solid acids such as bulk HPA, silica-supported HPA, Cs-HPA, zeolite HBEA, $SiO_2$–$Al_2O_3$ and Amberlyst 35W resin. Results showed that the reaction can be efficiently promoted on catalysts containing a high density of strong Brønsted acid sites such as HPA/$SiO_2$ and Amberlyst 35W. In contrast, the PS conversion was poorly promoted on Lewis acids such as $SiO_2$–$Al_2O_3$. We also observed [12] that the ionone isomer distribution depends not only on the catalyst acid site nature (Lewis or Brønsted) but also on the site concentration, in agreement with earlier work with homogeneous catalysts showing that the acid type, concentration and strength

* Corresponding author. Tel.: +54-342-4555279; fax: +54-342-4531068.
*E-mail address:* dicosimo@fiq.unl.edu.ar (J.I. Di Cosimo).

0926-860X/$ – see front matter © 2009 Elsevier B.V. All rights reserved.
doi:10.1016/j.apcata.2009.02.002

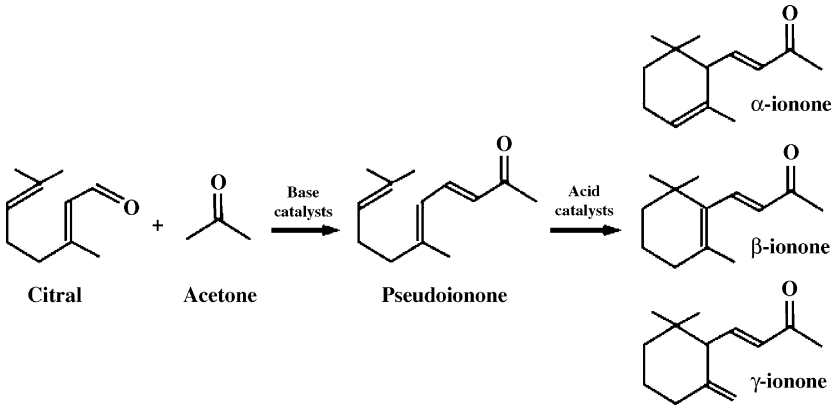


**Scheme 1.** Two-step process for ionone synthesis.

determine which ionone isomer will be preferentially obtained [15].

In this paper we continue our studies on the use of solid acid catalysts to selectively convert PS into ionones. Specifically, a series of HPA/$SiO_2$ catalysts with different HPA loadings was prepared and characterized by several techniques in order to determine the structural, textural and acidic properties of these materials. We investigated the effect of HPA loading on catalyst activity and selectivity and correlated them with the catalyst surface acidic properties. Furthermore, we studied the effect of the reaction temperature with the aim of improving the productivity to ionones and controlling the ionone isomer distribution (α, β and γ).

We also provide new insight into mechanistic aspects of the heterogeneously catalyzed reaction and postulate a reaction mechanism for this process that takes into account the different stability and reactivity of the three ionone isomers.

## 2. Experimental

### 2.1. Catalyst synthesis

Four silica-supported heteropolyacid catalysts with HPA loadings between 18.8 and 58.5 wt% were prepared by incipient wetness impregnation method. The tungstophosphoric acid ($H_3PW_{12}O_{40}.xH_2O$, Merck, GR) was added to a commercial $SiO_2$ (Grace Davison, G62, 99.7%, 272 $m^2/g$, pore diameter = 122 Å) using an aqueous solution of HPA. The stability of the $H_3PW_{12}O_{40}.xH_2O$ species in water was confirmed by UV–vis. Then, samples were dried at 353 K and finally decomposed and stabilized at 523 K for 18 h in $N_2$ flow. The resulting HPA-doped $SiO_2$ samples were denoted as HPAS.

### 2.2. Catalyst characterization

Structural properties of the solids were analyzed by X-ray diffraction (XRD) using a Shimadzu XD-D1 diffractometer equipped with Cu Kα radiation and a Ni filter. BET surface areas were determined by $N_2$ adsorption at 77 K using an Autosorb Quantachrome 1-C sorptometer.

The chemical content of HPA in HPAS catalysts was quantitatively analyzed by UV spectroscopy with a Metrolab 1700 UV–vis spectrometer following procedures described in the literature [16].

Catalyst acid site densities ($n_a$) were measured by temperature-programmed desorption (TPD) of $NH_3$ preadsorbed at 373 K. Samples (150 mg) were treated in He (40 $cm^3$/min) at 523 K for 1 h, cooled down to 373 K, and then exposed to a 1% $NH_3$/He stream during 15 min. Weakly adsorbed $NH_3$ was removed by flushing with He at 373 K during 1 h. Finally, the sample temperature was increased from 373 to 1073 K at a rate of 10 K/min in a He flow of 60 $cm^3$/min. Desorbed $NH_3$ was analyzed by mass spectrometry (MS) in a Baltzers Omnistar unit.

The chemical nature of surface acid sites was determined by Infrared Spectroscopy (IR) of pyridine using a Shimadzu FTIR Prestige-21 spectrophotometer. Experiments were carried out using an inverted T-shaped cell containing the sample wafer and fitted with $CaF_2$ windows. The absorbance scales were normalized to 20-mg wafers. Sample wafers were evacuated at 523 K, then cooled down to room temperature to take the catalyst spectrum. After exposure to 0.12 kPa of pyridine at room temperature samples were evacuated consecutively at 298, 373, 423 and 473 K and the resulting spectrum was recorded at room temperature. Spectra of the adsorbed species were obtained by subtracting the catalyst spectrum.

### 2.3. Catalytic testing

The cyclization of pseudoionone, PS (Fluka, >95%) was carried out at 343–383 K under autogenous pressure (≈250 kPa) in a batch Parr reactor, using dehydrated toluene as a solvent with typically a Toluene/PS = 71 molar ratio and a catalyst/PS = 56 wt% ratio. Catalysts were ground and sieved to produce <75 μm particles and then pretreated ex situ in a $N_2$ stream at 523 K for 2 h to remove adsorbed water. After introducing the reactant and solvent the reactor was sealed and flushed with $N_2$ and then the mixture was heated up to the final reaction temperature under stirring (300 rpm). Then the catalyst was added to the reaction mixture to start the reaction. Reaction products were periodically analyzed during the 6-hour reaction in a Varian Star 3400 CX gas chromatograph equipped with a FID and a Carbowax Amine 30 M capillary column. Main reaction products were ionones (α, β and γ isomers). Selectivities ($S_j$, mol of product $j$/mol of PS reacted) were calculated as $S_j = C_j/\Sigma C_j$ where $C_j$ is the concentration of product $j$. Yields ($\eta_j$, mol of product $j$/mol of PS fed) were calculated as $\eta_j = S_j\ X_{PS}$, where $X_{PS}$ is the pseudoionone conversion. Initial ionone formation rate ($r^0_{IONONE}$) was calculated from the initial slope of the $\eta_{IONONE}$ vs. time curve.

## 3. Results and discussion

### 3.1. Chemical, textural, structural and acid characterization of HPAS catalysts

The chemical composition, BET surface area and acid properties of the solid acids are presented in Table 1. The HPA loading in HPAS samples was varied between 18.8 and 58.5 wt%, according to quantitative measurements performed by UV spectroscopy.

Bulk commercial HPA had a low surface area value of 9 $m^2/g$. After impregnation of HPA on the high surface area silica (272 $m^2$/

**Table 1**
Physicochemical, textural and acid properties of $SiO_2$, HPA and HPAS catalysts.

| Catalyst | HPA loading[a] (wt%) | Monolayer coverage ($m^2$ HPA/$m^2$ $SiO_2$) | Surface area ($m^2$/g) | Surface acid properties | | | | |
|---|---|---|---|---|---|---|---|---|
| | | | | Acid site density | | Acid site nature[d] | | |
| | | | | $n_a$[b] (μmol/g) | $n_{H+}$ (μmol/g) | $B$ (area/g) | $L$ (area/g) | $B/(B+L)$ (%) |
| $SiO_2$ | – | – | 272 | 0 | – | 0 | 0 | 0.0 |
| HPAS-1 | 18.8 | 0.25 | 208 | 229 | 200[a] | 45 | 16 | 73.8 |
| HPAS-2 | 26.6 | 0.39 | 203 | 258 | 280[a] | 71 | 26 | 73.2 |
| HPAS-3 | 42.5 | 0.80 | 155 | 377 | 440[a] | 161 | 15 | 91.5 |
| HPAS-4 | 58.5 | 1.53 | 144 | 566 | 610[a] | 434 | 16 | 96.4 |
| HPA | – | – | 9 | 534 | 1040[c] | 473 | 0 | 100.0 |

[a] by UV spectroscopy analysis; [b] by TPD of $NH_3$; [c] calculated as $H^+$ per HPA unit; [d] by FTIR of pyridine adsorbed at 298 K and evacuated at 423 K (B: Brønsted sites; L: Lewis sites).

g), the resulting HPAS catalysts showed surface areas in the range of 144–208 $m^2$/g. The HPAS surface area decreased with increasing HPA loading, probably because of the formation of an incipient three-dimensional HPA structure that partially blocks the silica pores. This result was observed by XRD, as will be described in the next paragraph.

The XRD patterns of HPA, $SiO_2$ and HPAS samples are shown in Fig. 1. No crystalline HPA phase was detected on HPAS-1 and HPAS-2 which is in agreement with previous work showing that HPA is highly dispersed on silica samples containing HPA loadings below 30 wt%, [17]. For higher HPA loadings (samples HPAS-3 and HPAS-4), an incipient phase of $H_3PW_{12}O_{40}.xH_2O$ was observed. Consistently, calculations of HPA surface coverage carried out by considering that the heteropolyacid species after catalyst calcination is $H_3PW_{12}O_{40}.nH_2O$ ($n$ = 0.3–6.0) [18,19], indicate that the $SiO_2$ surface may be covered by one monolayer of HPA for HPA loadings of about 48 wt% (Table 1, column 3).

The surface acid properties of HPAS samples were investigated by combining TPD and infrared measurements of adsorbed $NH_3$ and adsorbed pyridine, respectively. We measured the $NH_3$ adsorption site densities and binding energies by TPD of $NH_3$ preadsorbed at 373 K. Fig. 2 shows the $NH_3$ desorption rate as a function of desorption temperature for $SiO_2$, unsupported HPA and HPAS samples. The total amount of desorbed $NH_3$ was measured by integration of the TPD curves of Fig. 2 and it was taken as an indication of the total acid site density, $n_a$. The resulting $n_a$ values are reported in Table 1. The proton contents ($n_{H+}$, μmol $H^+$/g cat) on HPAS samples were calculated from the HPA loadings measured by UV spectroscopy and considering that the heteropolyacid used was $H_3PW_{12}O_{40}$. The $n_{H+}$ values (Table 1, column 6) were similar to the corresponding $n_a$ values (μmol $NH_3$/g cat). This agreement between $n_a$ and $n_{H+}$ values indicates that the HPA protons are completely accessible for $NH_3$ adsorption, even on samples containing high HPA loadings. On the other hand, the $n_a$ value measured for unsupported HPA was similar to that of HPAS-4 sample, what suggests that only a part of the acid sites of the three-dimensional structure of bulk HPA is available for $NH_3$ adsorption.

On unsupported HPA, $NH_3$ desorbed in a single sharp peak at about 900 K, what reveals the strong acidity and energetic

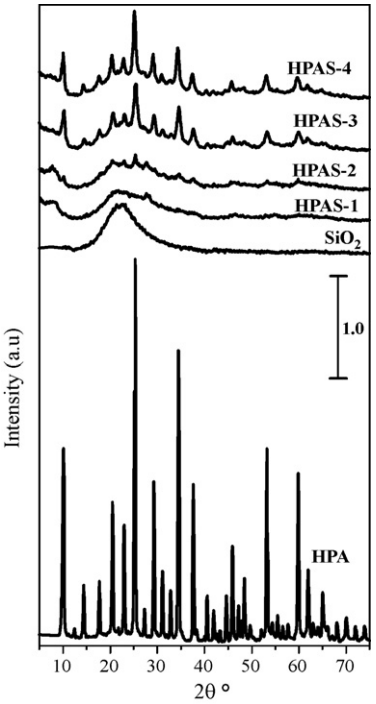


**Fig. 1.** XRD patterns of HPA, $SiO_2$ and HPAS samples.

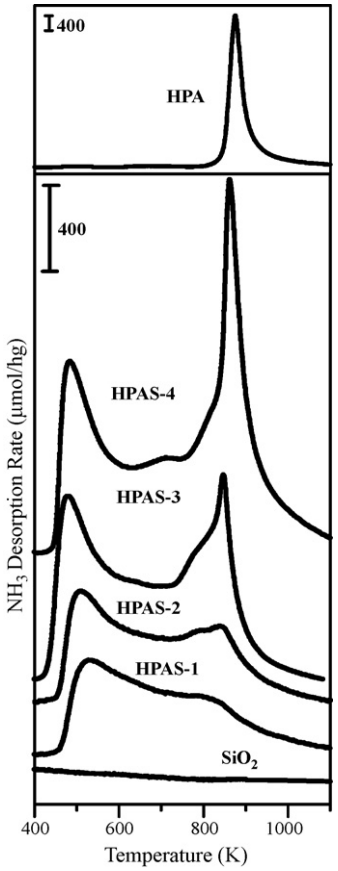


**Fig. 2.** TPD profiles of $NH_3$ on $SiO_2$, HPA and HPAS samples. $NH_3$ adsorption at 373 K, 10 K/min heating rate.

uniformity of the heteropolyacid protons. In contrast, the $NH_3$ desorption of HPAS samples gave rise to several desorption peaks at temperatures in the range of 500–900 K reflecting the presence of surface acid species that bind $NH_3$ with different strength. For low HPA loadings (20–40% of monolayer coverage), the broad strength distribution is probably the result of the HPA spreading on the silica surface that generates highly interacting heteropolyacid-support species. At higher HPA loadings a narrow high temperature peak develops and gradually approaches 900 K, indicating the preferential generation of strong acid sites, due to the increasing amount of HPA without interaction, as it was observed by XRD.

The chemical nature, strength and density of surface acid sites on HPAS catalysts were investigated by analyzing the FTIR spectra obtained after adsorption of pyridine at 298 K and evacuation at increasing temperatures. The FTIR spectra of adsorbed pyridine after evacuation at 423 K are shown in Fig. 3. No pyridine adsorption was detected on the silica support. Bulk HPA showed only the IR bands typical of pyridinium ion formed on Brønsted acid sites, i.e., the 8a–8b and 19b–19a ring vibrations modes at 1636, 1608, 1537 and 1485 $cm^{-1}$, whereas the pyridine spectra on the HPAS samples exhibited an additional weak band arising from pyridine coordinated on Lewis acid sites at ~1450 $cm^{-1}$ assigned to the 19b mode [20]. The fact that the HPAS samples displayed both Brønsted and Lewis acid bands suggests that upon impregnation of HPA on $SiO_2$, in addition to the Keggin structure that accounts for the Brønsted acid species, the heteropolyacid partially transforms giving rise to lacunary or unsaturated species [17] of Lewis acid character formed by interaction with the silica support.

A measure of the relative contribution of the Brønsted and Lewis acid sites of HPAS samples was obtained from Fig. 3 by integration of the bands at ~1540 and ~1450 $cm^{-1}$, respectively, corresponding to the 19b ring vibrations of pyridine [21]; results are presented in Table 1. It is observed that the area under the band corresponding to pyridine adsorbed on Brønsted acid sites increased with the HPA loading whereas that of Lewis acid sites remained unchanged. As a consequence, the relative contribution

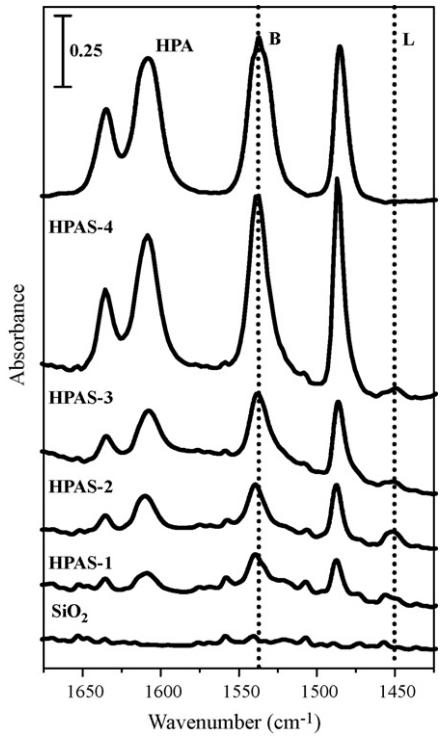


**Fig. 3.** FTIR spectra after pyridine adsorption at 298 K and evacuation at 423 K on HPA, $SiO_2$ and HPAS catalysts. B: Brønsted; L: Lewis.

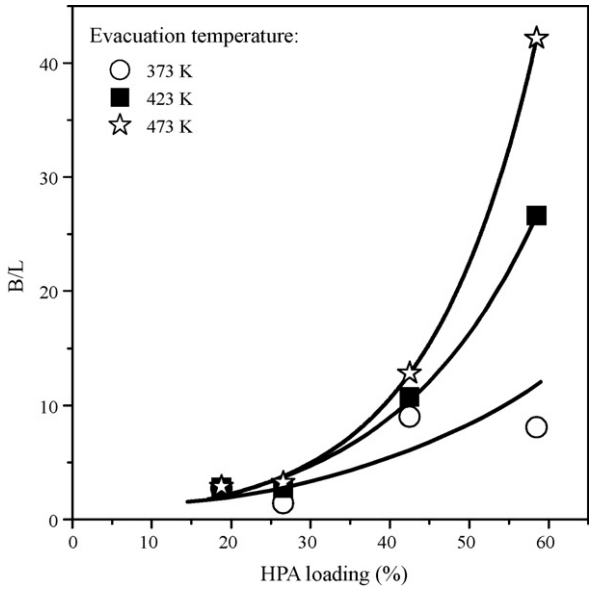


**Fig. 4.** Effect of the HPA loading and evacuation temperature on the Brønsted/Lewis acid site ratio (B/L). B/L ratio determined from FTIR of pyridine adsorbed at 298 K and evacuated at 373, 423 and 473 K on HPAS catalysts.

of Brønsted acid sites to the overall acidity, i.e., the B/(B + L) ratio, also increased with increasing the HPA loading. On the other hand, Fig. 4 shows that the Brønsted/Lewis ratio increased when the pyridine evacuation temperature was increased. This indicates that the Brønsted acid sites of HPAS samples are more strongly acidic than the Lewis acid sites and retain pyridine up to higher evacuation temperatures. In summary, the results obtained by FTIR of adsorbed pyridine show that increasing the HPA loading in HPAS samples enhances both the density of Brønsted acid sites and the sample average acid strength.

### 3.2. Catalytic experiments on HPAS catalysts

#### 3.2.1. Effect of the HPA loading

In a previous work we reported that the PS cyclization toward ionones is essentially promoted by strong Brønsted acid sites [14]. The acid site characterization shown in Table 1 and Figs. 2–4 indicated that the Brønsted acid sites represent more than 70% of the total acidity of the HPAS catalysts and that the contribution of the Brønsted acidity is enhanced at higher HPA loadings. Then, we decided to study here the effect of HPA content on the activity and selectivity of HPAS catalysts for PS cyclization. Catalytic tests were carried out using toluene as a solvent.

The catalytic activity of HPAS catalysts, $SiO_2$ and bulk HPA is compared at identical reaction conditions in Fig. 5a. The $SiO_2$ support was inactive for PS cyclization because it lacks of acidic properties (Table 1). On bulk HPA, the PS conversion after the 6-h run was only 4% (Fig. 5a) in spite of the fact that this sample contains the highest density of Brønsted acid sites (Table 1). This low activity of bulk HPA is explained by considering that the compact three-dimensional structure of HPA, with low specific surface area, impedes the access of the PS molecules to the active centers of the solid.

On HPAS catalysts, the PS conversion (Fig. 5a) increased with increasing the HPA loading, but curves tend to overlap as the HPA loading approaches the monolayer saturation coverage (~48 wt% HPA). For example, the PS conversion on samples HPAS-3 (42.5 wt% HPA) and HPAS-4 (58.5 wt%) after the 6-h runs were 88 and 93%, respectively. Even though the acid site density and strength increased continuously with the HPA loading (Table 1 and

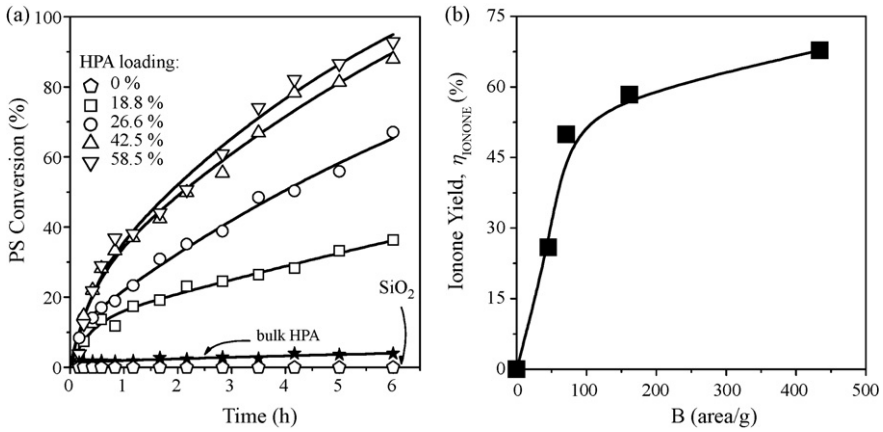


**Fig. 5.** Effect of the HPA loading. (a): PS conversion as a function of reaction time; (b): Ionone yield at $t$ = 6 h as a function of the Brønsted acid site band area (details in Table 1) [$T$ = 353 K, $n^0_{PS}$ = 0.009 mol, Toluene/PS = 71 (molar ratio), $W_{CAT}$ = 1.0 g].

Fig. 4), not all the acid sites seem to the available for the reaction at HPA coverages close to one monolayer. This effect is more evident in Fig. 5b where the ionone yields obtained with the HPAS catalysts are plotted against the corresponding Brønsted acid site band area (Table 1). It is observed that the ionone yield increased almost linearly with the Brønsted acid site band area for HPA loadings of up to about 30 wt%, but the curve tended to level off for higher HPA contents. This result probably reflects spatial constraints derived from stacking of heteropolyacid units for HPA loadings higher than 30 wt%, with the consequent hindering of the PS cyclization reaction that involves larger molecules than the $NH_3$ or pyridine probes.

The effect of the HPA loading was limited to the catalyst activity since in the experiments of Fig. 5, the selectivity to total ionones was independent of the HPA content reaching values between 72 and 75% after the 6-h runs. Thus, a final ionone yield as high as 68% was obtained on catalyst HPAS-4, which presented the highest conversion. Furthermore, the ionone isomer distribution on HPAS samples did not change with the HPA content when compared at similar PS conversion. For example, at a PS conversion of 36% the α:β:γ isomer ratio was 37:19:44 on all the HPAS samples of Table 1.

In spite of previous work showing that HPA is not soluble in non-polar aprotic solvents such as toluene [22], we decided to investigate the possible contribution of a homogeneously catalyzed pathway in our catalytic results by monitoring the presence of HPA in the liquid phase before and after reaction using sample HPAS-3. Fig. 6, curve (A) shows the UV–vis spectrum of the HPA impregnating aqueous solution used to prepare sample HPAS-3. This curve (A) presents the typical band at 260 nm corresponding to the Keggin anion of HPA [23]. When the HPAS-3 sample was immersed in toluene at 353 K, curve (B), the HPA signal was not detected in the toluene phase what indicates that HPA was not dissolved from sample HPAS-3. A spectrum similar to the latter was obtained when the reaction media was analyzed after reaction at 353 K on sample HPAS-3, curve (C). These results confirmed that HPA was not leached from sample HPA-3 during reaction and ruled out the contribution of any homogeneous pathway in our catalytic results.

### 3.2.2. Effect of the PS conversion and reaction time

Fig. 7 shows the results obtained on sample HPAS-3 at 353 K and typically illustrates the evolution of PS conversion ($X_{PS}$), total

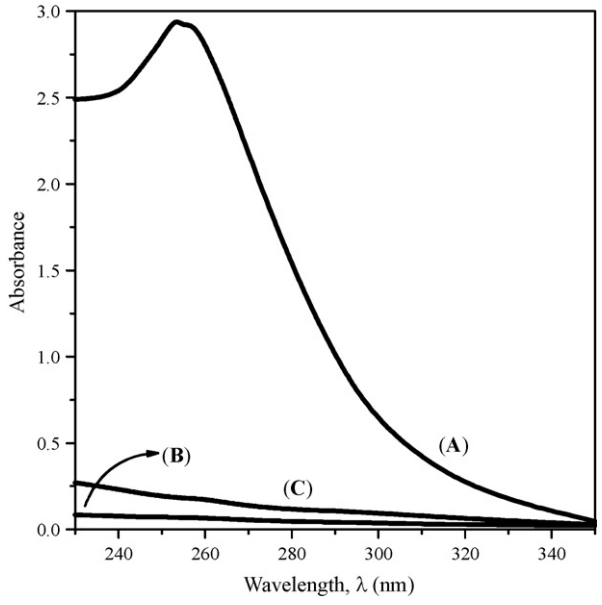


**Fig. 6.** Liquid-phase UV–vis spectra. (**A**): HPA impregnating aqueous solution; (**B**): 1.0 g of HPAS-3 in 70 mL of toluene at 353 K; (**C**): after reacting 2 mL of PS on 1.0 g of HPAS-3 in 70 mL of toluene at 353 K.

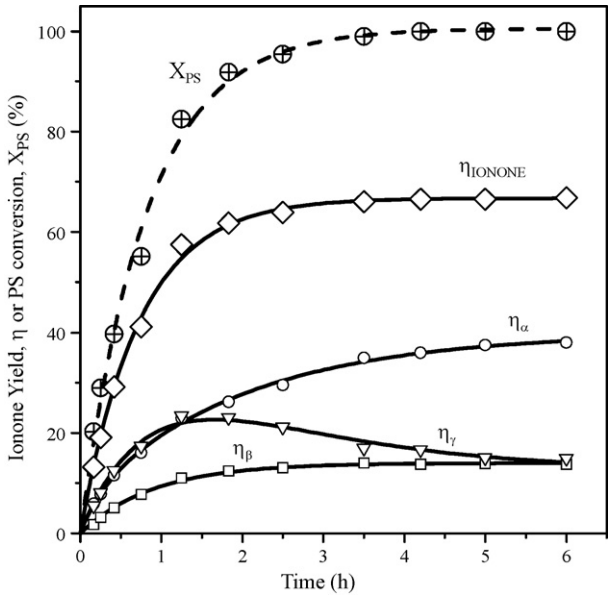


**Fig. 7.** PS conversion and ionone yields on HPAS-3. [$T$ = 353 K, $n^0_{PS}$ = 0.009 mol, Toluene/PS = 71 (molar ratio), $W_{CAT}$ = 2.0 g].

ionone yield ($\eta_{IONONE}$) and ionone isomers (α, β and γ) as a function of reaction time. The local slopes of the ionone yield curves in Fig. 7 give the rate of formation of each product at a specific PS conversion and reaction time. The nonzero initial slopes of the isomer yield curves indicate that the three ionones are primary products formed directly from PS.

The β isomer yield increased with time on stream reaching 14% when total PS conversion was achieved after 3.5 h; then, it remained constant until the end of the 6-h run. The shape of the β-ionone yield curve is consistent with direct formation from PS and no further transformation to other compounds; in other words, the β isomer is a primary and final product from PS. The stability of this isomer is attributed to the presence of the extended conjugated system in the molecule.

The α isomer yield curve monotonically grew with the reaction time whereas the γ isomer curve presented a maximum. These results indicate that γ-ionone is consecutively isomerized to the α isomer. This effect is even more evident at higher reaction times since after reaching 100% PS conversion (~3.5 h), $\eta_{IONONE}$ remained constant but formation of α-ionone at the expense of the γ isomer was clearly observed. Conversion of γ- into α-ionone is some way expected considering the instability of the former due to the exocyclic C=C bond (Scheme 1).

In summary, results of Fig. 7 show that the ionone isomer distribution changes with time on stream. The α isomer fraction continuously increases with reaction time, and becomes the main product at the end of the run at 353 K.

### 3.2.3. Effect of the reaction temperature

The effect of varying the reaction temperature on the catalytic performance of silica-supported heteropolyacid samples was investigated on catalyst HPAS-4. In Fig. 8 the ionone yields resulting from the PS cyclization in the range of 343-383 K are presented.

From the data of Fig. 8 we determined the initial ionone formation rate ($r^0_{IONONE}$, μmol/gh) by calculating the initial slopes according to

$$r^0_{IONONE} = \frac{n^0_{PS}}{W}\left[\frac{d\eta_{IONONE}}{dt}\right]_{t=0},$$

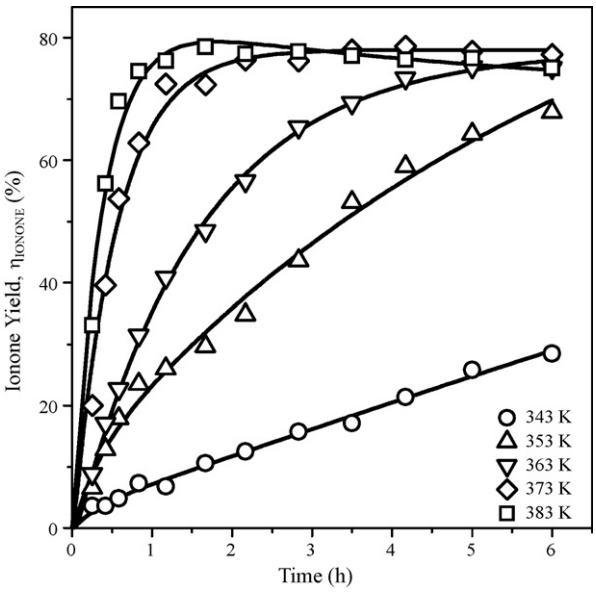


**Fig. 8.** Effect of the reaction temperature. Ionone yield as a function of the reaction time. [HPAS-4, $n^0_{PS}$ = 0.009 mol, Toluene/PS = 71 (molar ratio), $W_{CAT}$ = 1.0 g].

where $W$ is the catalyst weight and $n^0_{PS}$ is the initial mol of PS. A 18-fold enhancement of the initial ionone formation rate was observed when the reaction temperature was increased from 343 to 383 K on sample HPAS-4. In fact, the $r^0_{IONONE}$ values in μmol/hg were 991 at 343 K, 4480 at 353 K, 13,310 at 373 K and 18,280 at 383 K.

The reaction temperature had a significant effect not only on the initial ionone formation rate but also on the PS conversion and ionone yield. As a consequence, the ionone yield was only 29% at 343 K after the 6-h run but reached 79% at 383 K in 1.5 h. Also, complete conversion of PS was achieved in 5, 3.5, and 1.5 h at 363, 373, and 383 K, respectively. However, after reaching 100% PS conversion at 383 K, the ionone yield slightly decreased with time on stream (Fig. 8) thereby suggesting a slow ionone degradation at this temperature.

The evolution of ionone isomer yields as a function of reaction time at increasing reaction temperatures on sample HPAS-4 is presented in Fig. 9. The shape of the β-ionone yield curves was maintained as the temperature increased therefore indicating that β-ionone was not converted into the other isomers even at high reaction temperatures. The highest β-ionone yield, 18%, was obtained when reaching the complete PS conversion, i.e., after 3.5 h at 373 K and 1.5 h at 383 K. However, a slight β-ionone degradation with time was observed at 383 K.

Results of Fig. 9 also show that the α isomer yield continuously grew with time regardless of the reaction temperature. The highest α-ionone yield, 58%, was obtained at the end of the run at 383 K. The shape of the γ isomer curve, on the other hand, changed as the temperature increased; at low reaction temperatures (343 and 353 K) no maximum was observed in the time frame of the experiment due to the slower overall PS conversion rates whereas at higher temperatures, the maximum indicating γ- to α-ionone

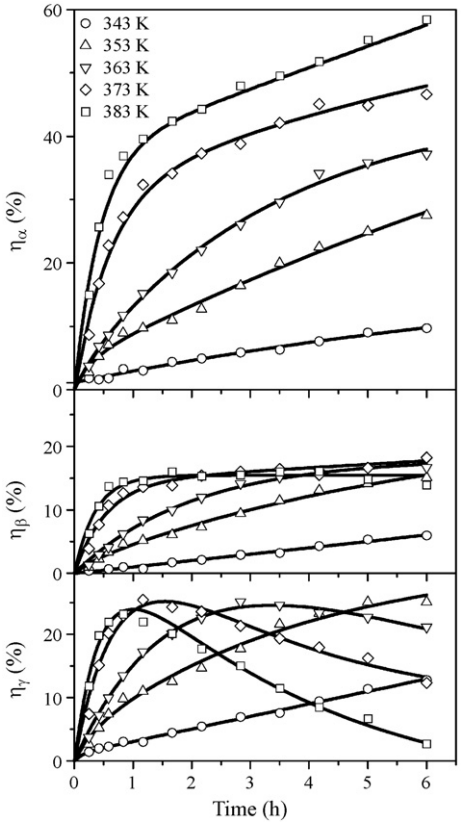


**Fig. 9.** Effect of the reaction temperature. Ionone isomer yields as a function of the reaction time. [HPAS-4, $n^0_{PS}$ = 0.009 mol, Toluene/PS = 71 (molar ratio), $W_{CAT}$ = 1.0 g].

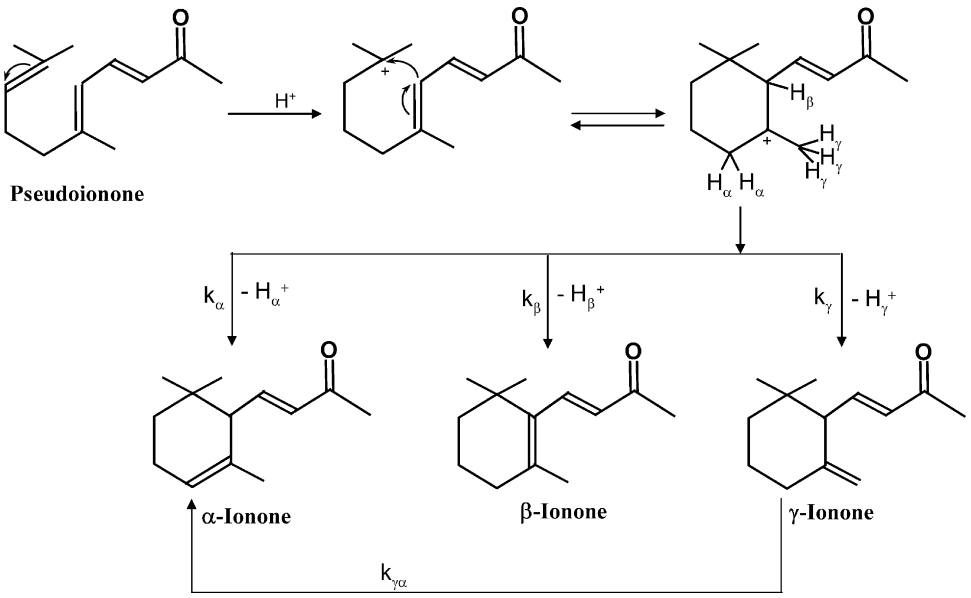


**Scheme 2.** Reaction pathways for ionone formation from PS on HPAS catalysts.

isomerization gradually shifted to lower reaction times. Thus, just a 2% residual γ-ionone yield was quantified at the end of the run at 383 K.

From the initial slopes of the yield vs. time curves of Fig. 9 we determined the initial formation rate of ionone isomers at different temperatures. Then, we calculated the corresponding apparent activation energies, $E_a$, by using the Arrhenius equation for the rate constants, $k = Ae^{-Ea/RT}$. The $E_a$ values obtained for the formation of α, β and γ isomers from PS were 24, 19 and 15 kcal/mol, respectively.

In addition, we determined the ionone isomer distribution at different temperatures and at 40% PS conversion, Fig. 10. It is observed that the fraction of α-ionone increases at the expense of γ-ionone at increasing temperatures, while the amount of β isomer remains almost unchanged. Data at lower or higher conversion levels showed a similar tendency. This ionone distribution trend with temperature is in agreement with the $E_a$ values determined from the initial formation rate of each ionone isomer.

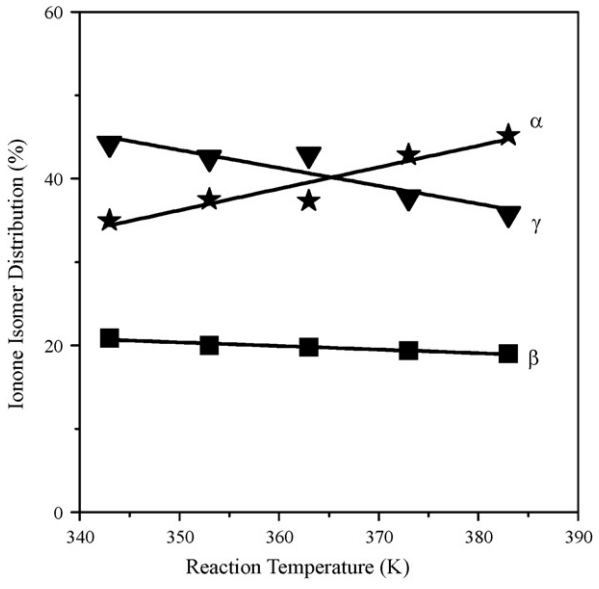


**Fig. 10.** Ionone isomer distribution as a function of the reaction temperature. [HPAS-4, $n^0_{PS} = 0.009$ mol, Toluene/PS = 71 (molar ratio), $W_{CAT}$ = 1.0 g, $X_{PS}$ = 40%].

In summary, results in Fig. 8 show that total ionone yields of 79% are obtained from PS on HPAS-4 sample after 1.5 h at 383 K or 3.5 h at 373 K using a reactant to catalyst weight ratio of 3. This ionone yield is comparable to those reported for the homogeneously catalyzed PS cyclization using concentrated sulfuric acid at low temperatures and high pressures using a reactant to catalyst weight ratio of 0.3 [4,5,6]. Although the commercial process produces mainly the β isomer, the use of environmentally friendly HPA-based solid catalysts opens a good perspective for the heterogeneous process as an alternative to sulfuric acid to synthesize ionones. Also, results of Figs. 9 and 10 indicate that the ionone isomer distribution may be controlled by properly selecting the temperature and the reaction time. In particular, the α:β:γ isomer ratio on HPAS-4 at 383 K changes from 54:20:26 at 1.5 h when total PS conversion is reached, to a product which contains about 80% α-ionone and 20% β-ionone with almost no γ isomer at the end of the 6-h catalytic run.

### 3.2.4. Reaction pathways

From the previous results of Figs. 7 and 9, the reaction pathways for the PS conversion to ionones on HPA/$SiO_2$ catalysts are postulated in Scheme 2. The PS molecule is activated on surface Brønsted acid sites forming a common cyclic intermediate for the consecutive ionone isomer formation. In this cyclic intermediate $H_\alpha$ (two), $H_\beta$ (one) and $H_\gamma$ (three) are the protons that have to be detached to form α, β and γ-ionone, respectively.

Taking into account the chemical structure of the ionone molecules, the following stability order for the ionone isomers can be speculated: β > α > γ-ionone. The three isomers are primary products formed directly from PS, but consecutive isomer interconversion is expected, in particular at high reaction temperatures due to the faster overall kinetics. The α isomer is formed not only from PS but also from double bond isomerization of the least stable γ isomer in a consecutive pathway. Contrarily, the β isomer forms exclusively from PS regardless of the reaction temperature and time. The β isomer is more difficult to obtain than the other ones and its formation would require the strongest surface acid sites. The stability of this isomer is provided by the extended conjugated system and explains the fact that β-ionone is not transformed in the other ionones by isomerization.

## 4. Conclusions

The liquid-phase cyclization of pseudoionone to ionones is efficiently promoted on silica-supported heteropolyacid catalysts. Pseudoionone conversion occurs on Brønsted acid sites and increases proportionately to the surface proton density until approaching the HPA content corresponding to the monolayer saturation coverage. For higher HPA loadings, stacking of HPA units hinders the pseudoionone cyclization because the proton acid sites become increasingly inaccessible for reactant adsorption and conversion. Consistently, unsupported HPA exhibits a very poor activity for converting pseudoionone.

Ionone isomers ($\alpha$, $\beta$ and $\gamma$) are primary products resulting from a common cyclic intermediate formed through pseudoionone protonation on a Brønsted acid site. The three isomers present different stability and reactivity so that the ionone isomer distribution can be controlled by changing the reaction conditions. In particular, the $\alpha$ isomer selectivity is enhanced at high reaction temperatures and times because of the transformation of the least stable $\gamma$-ionone in $\alpha$-ionone. At these conditions the $\alpha$ isomer is predominant, representing $\sim$80% of the total ionones. The most stable $\beta$ isomer is not consecutively transformed into other products and contributes up to 20% of the total ionones.

Ionone synthesis is favored at high reaction temperatures so that total ionone yields of about 79% are obtained on a 58.5 wt% HPA/$SiO_2$ catalyst at 383 K and 250 kPa in 1.5 h. This ionone yield is comparable to those reported for the homogeneously catalyzed ionone synthesis using concentrated sulfuric acid at subambient temperatures and high pressures.

## Acknowledgements

Authors thank the Agencia Nacional de Promoción Científica y Tecnológica (ANPCyT), Argentina (Grant PICT 14-11093/02), CONICET, Argentina (Grant PIP 5168/05) and the Universidad Nacional del Litoral, Santa Fe, Argentina (Grant CAI + D 007-040/05) for the financial support of this work. They also thank Prof. P. E. Mancini for useful discussions and H. Cabral for technical assistance.

## References

[1] Ullmann's Encyclopedia of Industrial Chemistry, Sixth edition, 2002. (electronic).
[2] E. Brenna, C. Fuganti, S. Serra, P. Kraft, Eur. J. Org. Chem. (2002) 967.
[3] H. Hibbert, L.T. Cannon, J. Am Chem. Soc. 46 (1924) 119.
[4] O. Hertel, H. Kiefer, L. Arnold, US Patent 4 565 894 (1986), to BASF Aktiengesellschaft.
[5] U. Rheude, U. Horcher, D. Weller, M. Stroezel, US Patent 6 288 282 (2001), to BASF Aktiengesellschaft.
[6] K. Steiner, H. Ertel, H. Tiltscher, US Patent 5 453 546 (1995), to Hoffmann-La Roche Inc.
[7] G. Ohloff, G. Schade, Angew. Chem. Internat. Ed. 2 (1963) 149.
[8] V.K. Díez, C.R. Apesteguía, J.I. Di Cosimo, J. Catal. 240 (2006) 235.
[9] S. Abelló, F. Medina, D. Tichit, J. Pérez-Ramírez, X. Rodríguez, J.E. Sueiras, P. Salagre, Y. Cesteros, Appl. Catal. A: General 281 (2005) 191.
[10] C. Noda Pérez, C.A. Henriques, O.A.C. Antunes, J.L.F. Monteiro, J. Molec. Catal. A: Chem. 233 (2005) 83.
[11] M.J. Climent, A. Corma, S. Iborra, K. Epping, A. Velty, J. Catal. 225 (2004) 316.
[12] D. Guo, Z.-F. Ma, Q.-Z. Jiang, H.-H. Xu, Z.-F. Ma, W.-D. Ye, Catal. Lett. 107 (2006) 155.
[13] Z. Lin, H. Ni, H. Du, C. Zhao, Catal. Comm. 8 (2007) 31.
[14] V.K. Díez, C.R. Apesteguía, J.I. Di Cosimo, Cat. Lett. 123 (2008) 213.
[15] E.E. Royals, Ind. Eng. Chem. 38 (1946) 546.
[16] H. Freund, M.L. Wright, R.K. Brookshier, Anal. Chem. 23 (5) (1951) 781.
[17] I.V. Kozhevnikov, K.R. Kloetstra, A. Sinnema, H.W. Zandbergen, H. van Bekkum, J. Molec. Catal. A: Chem. 114 (1996) 287.
[18] N. Mizuno, M. Misono, Chem. Rev. 98 (1998) 199.
[19] M.S. Kaba, M.A. Barteau, W.Y. Lee, I.K. Song, Appl. Catal. A: General 194-195 (2000) 129.
[20] C. Morterra, A. Chiorino, G. Ghiotti, E. Fisicaro, J. Chem. Soc. Faraday Trans. I 78 (1982) 2649.
[21] B. Bachiller-Baeza, J.A. Anderson, J. Catal. 228 (2004) 225.
[22] I.V. Kozhevnikov, Chem. Rev. 98 (1998) 171.
[23] M. Kimura, T. Nakato, T. Okuhara, Appl. Catal. A: General 165 (1997) 227.